Redundant Mechanisms for Stable Cell Locomotion Revealed by Minimal Models

Charles W. Wolgemuth,[†‡*] Jelena Stajic,[‡] and Alex Mogilner[§¶]
[†]Department of Cell Biology and [‡]Center for Cell Analysis and Modeling, University of Connecticut Health Center, Farmington, Connecticut; and [§]Department of Mathematics and [¶]Department of Neurobiology, Physiology, and Behavior, University of California, Davis, California

ABSTRACT Crawling of eukaryotic cells on flat surfaces is underlain by the protrusion of the actin network, the contractile activity of myosin II motors, and graded adhesion to the substrate regulated by complex biochemical networks. Some crawling cells, such as fish keratocytes, maintain a roughly constant shape and velocity. Here we use moving-boundary simulations to explore four different minimal mechanisms for cell locomotion: 1), a biophysical model for myosin contraction-driven motility; 2), a G-actin transport-limited motility model; 3), a simple model for Rac/Rho-regulated motility; and 4), a model that assumes that microtubule-based transport of vesicles to the leading edge limits the rate of protrusion. We show that all of these models, alone or in combination, are sufficient to produce half-moon steady shapes and movements that are characteristic of keratocytes, suggesting that these mechanisms may serve redundant and complementary roles in driving cell motility. Moving-boundary simulations demonstrate local and global stability of the motile cell shapes and make testable predictions regarding the dependence of shape and speed on mechanical and biochemical parameters. The models shed light on the roles of membrane-mediated area conservation and the coupling of mechanical and biochemical mechanisms in stabilizing motile cells.

INTRODUCTION

Eukaryotic cells crawl by making protrusions, contracting their cytoskeletons, and adhering to the surrounding environment in a diverse, complexly controlled and integrated sequence of events (1). Biophysical and biochemical processes combine to produce motile cells that can track down pathogens, determine organism development, repair wounds, and allow cancerous cells to metastasize (2). Diverse experimental research using biochemistry, microscopy, genetics, and biophysics has produced a wealth of data that describe the molecular pathways of cell migration, the interconnectivity of the networks involved in transport and turnover of the cytoskeleton, and the forces and flows that are produced inside the cell (3). Yet, our understanding of how these processes unite to produce a crawling cell is still incomplete. One major missing link is comprehensive quantitative models that can predict the shape, speed, and intracellular processes of a moving cell (4).

Here we focus on the best-understood process, lamellipodial motility of cells on flat surfaces (5,6), and do not discuss other, equally important, modes of locomotion (1,7). We address the question of how motile cells maintain their shape and speed, the significance of which is underscored by the fact that cell shape reflects various dynamic cellular processes, such as remodeling of the cytoskeleton underlined by biochemical signaling (8). Roughly speaking, the question about cell shape and speed breaks into the following queries: How does the rear retract to keep up with the protruding front? How are the sides contained from spreading and collapsing (Fig. 1)? We can best address these questions by considering rapidly and steadily crawling simple-shaped cells such as fish epithelial keratocytes. When single cells are placed on a flat surface, they assume a stereotypical half-moon shape with a broad, flat, motile appendage, the lamellipodium, and maintain nearly constant cell shape, speed, and direction (Fig. 1) over many cell lengths (5,6). Lee et al. (9) proposed a geometric principle for lamellipodial shaping in motile keratocytes whereby the cell boundary expands at the front and retracts at the rear in a locally normal direction with spatially graded rates, so that the advancement at the front is the fastest, and then smoothly decreases toward the sides. A simple trigonometric formula can be used to determine cell shape as a function of the expansion/retraction rates, but the mechanics and biochemistry behind this cell shape remain to be determined.

In this work, we use moving-boundary simulations to model cell-shape dynamics. There is a rich history of investigators using such models to reproduce cell shape. Conceptually, one of the simplest models is one in which local stimulation and global inhibition of protrusive activity govern the local boundary velocity (10). Stéphanou et al. (11) added specific biophysics to the general model of Satulovsky et al. (10) by suggesting that membrane protrusions are induced by hydrostatic pressure and are opposed by tension from the actin filaments linked to the membrane and actomyosin contractility. The multiscale model of Rubinstein et al. (12) solved partial differential equations to describe the mechanics of an elastic actomyosin shell on the free boundary domain and reproduced the half-moon keratocyte shape. Another model considered the complex dynamics of two types of actin networks and reproduced the keratocyte shape by using moving-boundary

Submitted February 7, 2011, and accepted for publication June 15, 2011.

*Correspondence: cwolgemuth@uchc.edu

Editor: Leah Edelstein-Keshet.

© 2011 by the Biophysical Society

0006-3495/11/08/0545/9 $2.00

doi: 10.1016/j.bpj.2011.06.032

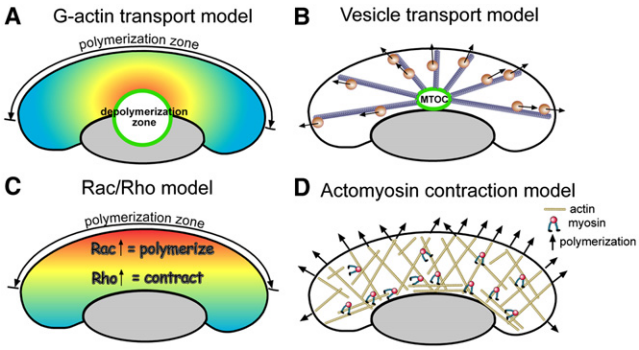

FIGURE 1 Schematic illustrations of the four cell motility models examined in this work. (*A*) G-actin transport to the leading edge creates graded protrusion of the F-actin cytoskeleton. (*B*) Delivery of new cell membrane via microtubule-assisted vesicle transport controls the rate of protrusion at the leading edge. (*C*) The RhoGTPases Rac and Rho regulate protrusion (Rac) and contraction (Rho) within the cell. (*D*) Myosin binds to and contracts the actin cytoskeleton, creating cytoskeletal flows that redistribute the bound myosin.

simulations (13). The three-dimensional computations of Herant and Dembo (14) employed reactive interpenetrating flow theory, which considers the actin polymer network to be a very viscous fluid that moves through the fluid cytoplasm. The role of biochemical signaling in cell shaping was highlighted by Marée et al. (15), who demonstrated that the reactions and diffusion of Rho GTPases can provide robust maintenance of a steady, rapidly motile keratocyte shape. Another model, similar in spirit to that of Marée et al. (15), was also shown to reproduce keratocyte shapes (16).

All of these studies were very useful in elucidating plausible motile cell dynamics; however, they used different techniques, considered only a single mechanism of lamellipodial motility, and were either schematic (10,11) or very complex and elaborate (12,14–16). There are many indications that redundant mechanisms underlie cell motility (3,8,17), so we set out to examine whether different mechanisms can maintain similar shapes and movements, and whether they can complement each other in this task. We did this within a unified and conceptually simple framework of a level set-based, finite-volume method (18). Based on the introductory notes above, we investigated the dynamics, shape, and speed of cells that result from four simple models for cell motility.

We begin with a G-actin transport-limited model based on the idea that actin monomer depletion leads to graded G-actin concentration and therefore to graded F-actin growth. We test whether this mechanism can define the cell shape. Then, we investigate whether delivery of membrane components via microtubules as a part of a polarized endo/exocytotic cycle (19) can account for the stable motile cell shape. Third, we examine a hypothesis that feedback between two RhoGTPases, Rac and Rho, leads to a mutually exclusive assembly of two different kinds of dynamic cytoskeletal structures, which in turn promotes the establishment of a front–back polarity and stable cell locomotion. Fourth, we quantitatively test the hypothesis that myosin contraction of the actin network is the predominant mechanism for cell motility, i.e., that myosin molecules are swept to the rear of the cell and generate a centripetal actin flow that pulls the rear forward and contains the sides, thereby shaping the lamellipodium. We also study the roles played by membrane area constraint and front–back polarity in shaping the cell. Finally, we test whether some of the four proposed mechanisms can complement each other in stabilizing cell shape. (Further details regarding the motivation for these models are presented in the Supporting Material.)

Below, we report that numerical simulations of the models demonstrate that the G-actin, microtubule, and Rac/Rho models can reproduce stable lamellipodial shape and movement. On the other hand, by itself, the model that treats myosin contraction of the actin network as the predominant mechanism for cell motility cannot reproduce cell shape robustly, but together with either a graded actin treadmill or the Rac/Rho-regulation model, it can capture many features of keratocyte motility. Therefore, we propose that some of the underlying complexities of the biochemical and biophysical mechanisms of cell motility can provide the necessary redundancy for robust cellular migration.

MATERIALS AND METHODS

In this section, we provide a qualitative description of the four motility models examined in this work. The mathematical details of the models are provided in the Supporting Material.

G-actin transport model

We start from one of the simplest possible mechanisms that can explain the shape and speed of a crawling cell: diffusion of G-actin from the rear, where F-actin disassembles, to the front and sides, where F-actin assembles (20) (Fig. 1 *A*). The idea that this is the limiting step in motility was previously explored in a limited and simplified form, in one dimension (21), but has not been proposed before to explain two-dimensional cell shape. To explore the crawling behavior predicted by this hypothesis, we constructed a model in which G-actin diffuses through the cell with diffusion coefficient D. We assume that the cell is polarized before motility occurs, i.e., a biochemical process inside the cell (e.g., as in the Rac/Rho model described below) activates polymerization at the leading edge of the cell and inhibits polymerization away from this region. Along the leading edge, F-actin grows at the rate $k_{on}g(x)$ (21) in proportion to the local G-actin concentration $g(x)$, where k_{on} is the polymerization constant. In the frame of the moving cell, the F-actin flows to the rear at the cell front and inwardly at the cell sides (12,22,23), and disassembles around the focal point to which the flow converges, largely in the region of the cell body, which is observed to be at the center of the cell rear. To account for this behavior, we define a circular region at the rear of the cell where F-actin disassembles at a constant rate, releasing monomeric G-actin, which then diffuses back to the leading edge. For simplicity, we do not consider nucleotide exchange on G-actin and reactions with thymosin and cofilin (24). The circular depolymerization zone moves with the cell rear, being pulled forward by the retracting cell membrane. We define the zone at the rear of the cell where actin does not polymerize in an ad hoc way, introducing a wide ellipse that is centered at the same location as the depolymerization zone. The location of that center moves with the center of the

depolymerization zone. Any boundary points that fall within the ellipse have a polymerization rate equal to zero; all other boundary points expand with the rate $\alpha k_{on} g(x)$. In addition, we assume that the cell has a preferred area A_0 and that deviations from this area produce an effective restoring velocity that is locally normal to the cell boundary. The rationale for this assumption stems from the hypothesis (25) that the plasma membrane is stretched tight around the lamellipodium. Thus, growing actin filaments at the leading edge push the membrane forward and to the sides, generating membrane tension. This tension retracts the membrane and F-actin remnants at the rear, keeping the area constant, as observed previously (25).

Microtubule-associated vesicle transport model

The polymerizing actin network can grow forward against the membrane in several different ways. For example, excess membrane can be preserved in folds, or the membrane envelope can slide forward effortlessly in synchrony with the cell crawling (26). In both cases, the lamellipodial area can be preserved such that any advance of the leading edge will be strongly coupled to retraction of the rear (25). In the model described above, we tested the latter assumption. Here, we assume that the membrane hinders the advance of the actin network, and, in accordance with data from Howes et al. (27), that exocytosis of vesicles transported to the leading edge creates excess space that allows polymerization to protrude the leading edge. We also assume that the membrane is simultaneously removed at the rear. The membrane tension-mediated feedback assumed in the model ensures that the total plasma membrane area is conserved, so the membrane area inserted into the leading edge is immediately internalized at the rear. The cell rear is effectively hauled forward by recycling the membrane from the rear. Thus, we assume that the flux of membrane vesicles to the leading edge is rate-limiting for the protrusion and is set by the density of the microtubule ends that are in close proximity to the membrane (Fig. 1 *B*). To the best of our knowledge, a quantitative model such as this has not been proposed before. Microtubules originate at the microtubule organizing center (MTOC) and grow radially outward. Because the MTOC is located in front of the nucleus, microtubules are partially occluded from the rear of the cell, as indicated by many previous observations (28). Therefore, the position of the MTOC with respect to the nucleus naturally defines a polarity for the cell. Thus, the polarity mechanism, as in the previous model, is upstream of the motility and shaping mechanism examined here. The nature of the polarity mechanism is largely unknown; however, some plausible hypotheses are discussed elsewhere (28). The density of the microtubule ends that reach the cell periphery depends on the kinetic parameters of the microtubule dynamics and the radial distance from the MTOC to the cell periphery. We assume that the rate of extension along the edge is proportional to the flux of membrane vesicles, which in turn is proportional to the local microtubule end density at the edge.

Rac/Rho model

The Rho GTPases Cdc42, Rac, and Rho are strongly implicated in determining cell polarity and regulating cell motility. Activation of Rac leads to the formation of lamellipodia and membrane ruffles (29), and Rac has been shown to be upstream of actin polymerization (30). On the other hand, Rho activation produces stress fibers and focal adhesions (31), and Rho is known to act upstream of myosin light chain kinase, which induces myosin contraction of the actin network (32). Therefore, a possible model for cell polarity and motility is one in which Rac activation leads to polymerization at the leading edge of the cell, and Rho activation at the rear of the cell induces myosin contraction of the cytoskeleton, which hauls the rear of the cell forward (Fig. 1 *C*). We simulate this mechanism using a simple reaction-diffusion model that was previously proposed for Rho GTPase dynamics (33). In this model, the activated GTPase positively regulates its own production, whereas deactivation occurs at a basal rate. Because the activated protein binds to the membrane, diffusion of the active form is two orders of magnitude slower than the diffusion of the cytosolic inactive form. We use this model to describe the dynamics of Rac and Rho and their effect on cell motility. Because this model is known to spontaneously polarize for one-dimensional fixed geometries, it is possible that the dynamics of these proteins can lead to stable, directed migration. We assume that active Rac induces actin polymerization. Active Rho induces myosin contraction, and we assume that the active form of Rho mirrors activated Rac. This model is conceptually similar to but mathematically simpler than that proposed by Marée et al. (15).

Actomyosin contraction model

Finally, we consider a mathematically more complex model in which actomyosin contraction of the cytoskeleton aids actin polymerization as the predominant mechanism underlying motility (Fig. 1 *D*). Measurements of the response of the actin cytoskeleton in living cells show that applied force causes the actin network to flow like a fluid on timescales longer than a few seconds (34). Therefore, we treat the cytoskeleton as a viscous fluid with viscosity η. We assume that myosin molecules can bind and unbind from the actin, with rate constants K_{on} and K_{off}, respectively. While it is bound, myosin is assumed to exert an isotropic, contractile stress on the actin network that is proportional to the local concentration of bound myosin. This leads to a flow of the cytoskeleton that pulls the bound myosin with it. Unbound myosin rapidly diffuses and is therefore treated as being uniform throughout the cell. We model the interaction between the cytoskeleton and the substrate as a resistive drag force that is proportional to the velocity of the cytoskeleton. F-actin polymerizes at the cell boundary. In keratocytes, the myosin at the rear of the cell acts to bundle the actin, which aligns parallel with the cell membrane (20,35). Therefore, there are fewer barbed ends in contact with the membrane, and the polymerization rate is decreased. We model this by assuming that the polymerization rate at the cell membrane decreases with increasing myosin concentration. Our model is similar to that of Barnhart et al. (23); however, the latter was not simulated fully with a moving boundary. We assume that the cell area is restored to the preferred one by an internal pressure that works to preserve a roughly constant cell volume. We also considered two extensions of this model: First, we added graded actin protrusion to the actomyosin contraction model, in similarity to previously proposed hypotheses (23). Specifically, we redefined the boundary velocity of the actomyosin contraction model by making the constant actin polymerization rate a function of the angular coordinate θ (from the cell center-of-mass): $V_p(\theta) = 1 + \beta \cos\theta$, where β is a constant. Second, we assumed that the actin protrusion rate is proportional to the concentration of active Rac, and the myosin stress is proportional to the concentration of active Rho.

RESULTS

For all of the models considered here, we studied the dynamics of an initially circular cell driven by the prescribed mechanisms. We then investigated the dependence of cell shape and speed on the parameters of the different models. The reader can best appreciate the evolution of the stable motile cell shapes by viewing the movies in the Supporting Material.

Robust motile cell shape can be stabilized by the G-actin transport mechanism

The G-actin transport model depends on three different parameters: the assembly rate constant at the leading edge, the disassembly rate of the F-actin, and the diffusion

coefficient of the G-actin. The diffusion coefficient can be scaled out of the problem, leaving just the dimensionless assembly and disassembly rates as free parameters. We simulate an initially circular-shaped cell with a uniform concentration of G-actin. The G-actin concentration is then depleted at the front of the cell and grows in the depolymerization zone. Points on the leading edge of the cell that are closer to the depolymerization zone receive a larger flux of G-actin, and thus polymerization is faster at these locations. At early times, faster polymerization occurs at the sides of the cell, which are closer to the rear, and the cell widens. The cell rear is pulled forward due to the conservation of cell area. As the rear of the cell moves forward, the depolymerization zone moves closer to the front of the cell, and eventually the cell front gets closer to the rear than the sides. Thus, the G-actin concentration is higher at the front than at the sides, and the front protrudes faster than the sides (Fig. 2, *A–C*). The geometric principle of shaping (9) ensures that the stable lamellipodial shape is a half disc with wings that protrude rearward (Fig. 2 *C*). This qualitative shape and its quantitative aspect ratio are very similar to those of keratocyte cells. The shape is not sensitive to any of the model parameters.

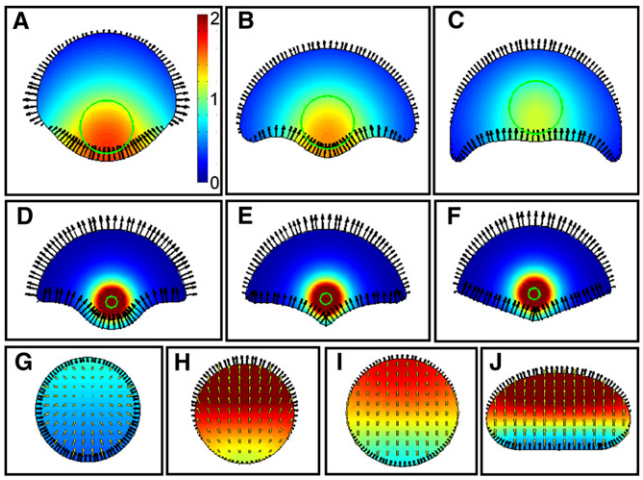

FIGURE 2 (*A–C*) Time series of the G-actin transport model, showing a time point shortly after the beginning of the simulation (*A*), an intermediate time point (*B*), and the stable crawling shape (*C*). The cell starts as a circle and contracts at the rear as the front moves forward. The steady-state shape is a half-disk with wings off the sides. This shape is nearly independent of the parameters. The color map shows the G-actin concentration in dimensionless units; arrows show the boundary velocity (Movie S1). (*D–F*) Time series of the microtubule-associated vesicle transport model. The cell starts as a circle and contracts at the rear as the front moves forward. The steady-state shape is fan-shaped, and this shape is nearly independent of the parameters. The color map shows the microtubule density; black arrows show the boundary velocity, and the green circle is the MTOC (Movie S2). (*G–J*) Time series of the Rac/Rho model. (*G–I*) Early dynamics show that the cell shrinks and then flips into the active state. (*J*) At long time periods, the cell takes on an elliptical/half-moon shape. The color map shows the concentration of species *a*; black arrows show the boundary velocity, and yellow arrows show the cytosolic velocity (Movie S3).

If F-actin disassembly increases, a larger pool of G-actin forms in the cell. Because the polymerization rate at the leading edge is proportional to the concentration of G-actin, the stable crawling speed of the cell is proportional to the magnitude of the source term (Fig. S1). Of interest, the crawling speed is nearly independent of the actin polymerization rate. This is because the rate at which the edge advances is proportional to the polymerization rate, but the pool of G-actin is depleted proportionally to the F-actin polymerization rate. These two effects compete against each other to make speed independent of the assembly rate. Cell speed in the G-actin transport model is proportional to the actin disassembly rate, which is along the lines of the effect observed by Cramer (36). These results regarding shape and speed are not counterintuitive; however, it is essential to obtain them by mathematics.

The microtubule-associated vesicle transport mechanism can also support a stable motile cell shape

Simulations of the microtubule-associated transport model produce a fan-shaped crawling cell (Fig. 2, *D–F*) characteristic of motile keratocytes. The shape and its aspect ratio are not strongly affected by the parameters. Note that the discontinuity in the boundary velocity at the corners of the resulting fan-like shape, which occurs at the point that microtubules cannot pass due to the cell body occlusion, is the cause of the sharp corners at the cell sides. The two main parameters of the model are an effective velocity that describes the membrane transport velocity multiplied by a probability factor for the membrane delivery, $\gamma = V_0 N \nu / 2\pi(\nu_+ + \nu_-)$, and the magnitude of the effective membrane area-restoring term, B. Not surprisingly, the crawling speed of the cell is linear in γ (Fig. S2 *A*). For values of the area-restoring term $B > 1$, the speed is constant; however, the speed goes to zero with B when $B < 1$ (Fig. S2 *B*). Thus, area preservation is essential for this mechanism to work. If the rear is allowed to slack off, the cell boundary moves farther from the leading edge, membrane delivery slows down, and the protrusion decreases.

The Rac/Rho model predicts a stable motile cell shape without the area conservation term, but not with it

As observed in a previous study (33), we find that cells will spontaneously polarize; therefore, the Rac/Rho model does not require an upstream polarization mechanism. We considered an initial condition with a uniform concentration of inactive protein and a nearly constant concentration of active protein. If the active protein concentration is perturbed with a random initial condition, the direction of polarization will be random, as expected from previous results (33). We also considered an initial concentration

that was perturbed with a small constant gradient. This initial cell state polarizes along the gradient direction and reaches steady state more quickly than when a random initial condition is used. The steady-state shape and speed are not affected by our choice of initial condition. Therefore, for most of our simulations, we perturbed the active protein concentration with a small uniform gradient.

We considered two separate scenarios: a cell with a preferred area and a cell with no preferred area. We found that when the cell area is not fixed, the cell initially begins to shrink (Fig. 2 *G*) because the concentration of active protein is below the threshold value. Therefore, myosin contraction driven by Rho exceeds the polymerization velocity produced by active Rac. As the cell shrinks, Rac at the front of the cell flips into the higher stable concentration, which causes the front of the cell to begin polymerizing faster than the myosin-induced contraction (Fig. 2, *H* and *I*). The cell eventually reaches a stable crawling shape with a high concentration of active Rac (low concentration of active Rho) at the front of the cell and a low concentration of active Rac (high concentration of active Rho) at the rear of the cell (Fig. 2 *J*). The velocity of the cell and the cell area are both proportional to the total protein concentration (Fig. S3); however, the cell shape is not strongly influenced by the total protein concentration, as the aspect ratio is relatively constant. It is somewhat unexpected that the aspect ratio of the cell is such that the cell is wider in the direction perpendicular to the direction of motion, because energetic considerations suggest that the system would evolve to a state that would minimize the length of the transition zone between the active and inactive states. However, in our system, the velocity of the boundary motion is proportional to the concentrations of active Rac and Rho. Because the polymerization rate is roughly constant on either side of the transition zone, the boundary dynamics favors a cell shape that is wider along the direction of the transition zone.

Of interest, if the cell area is fixed, the cell is no longer capable of achieving stable locomotion. As before, the cell still polarizes and begins to crawl. However, the rear of the cell eventually gets too close to the front of the cell, which causes the Rac at the rear of the cell to flip into the highly active stable state. The entire cell then has a uniform distribution of active Rac. The lack of polarization prevents further motion. We describe the implications of these results in the Discussion.

The actomyosin contraction mechanism alone does not stabilize the cell

Nondimensionalization of the actomyosin contraction model leads to four dimensionless parameters that influence the overall behavior of the model: the myosin-binding rate K_{on} and the myosin-off rate K_{off}, both of which are multiplied by the characteristic time L/V_0 ($f = \sigma_0 M_T/\Omega$, where $\sigma_0 M_T/L^2$ is the characteristic magnitude of the myosin-generated stress, $\Omega = \zeta V_0 L^3$ is the characteristic adhesion drag stress multiplied by the cell area, and $\varepsilon = \eta/\zeta L^2$ is the squared ratio of the characteristic length $(\eta/\zeta)^{1/2}$ on which the actin flow is induced by local myosin contraction to the cell size). To account for the bundling of actin by myosin, we assumed that bundled actin polymerizes more slowly at the leading edge and defined a parameter α that determined the reduction of protrusion by myosin. We chose typical values of these parameters to be $K_{on} = 0.25$, $K_{off} = 0.5$, $\sigma_0 = 0.2$, $\eta = 0.2$, and $\alpha = 1$, and investigated the behavior of the model near these typical values. We used an initial condition with a nearly uniform distribution of bound myosin that was perturbed by a small constant gradient between the front and back of the cell. We found three different behaviors for the evolution of the cell morphology. First, for small values of the myosin contractile stress ($f \leq 1$), the cell remains circular and there is flow of actin toward the center of the cell (Fig. 3 *A*), in agreement with previous observations of keratocyte fragments (37,38). For larger values of the myosin contractile stress, F-actin is rapidly pulled into the center of the cell, which produces a large concentration of myosin at the center. The small asymmetry in the cell shape that is produced by the initial conditions causes the cell to pinch in the center (Fig. 3 *B*). The third morphology arises when the viscosity is small compared with the substrate drag ($\varepsilon << 1$) and myosin strongly inhibits protrusion at the cell membrane.

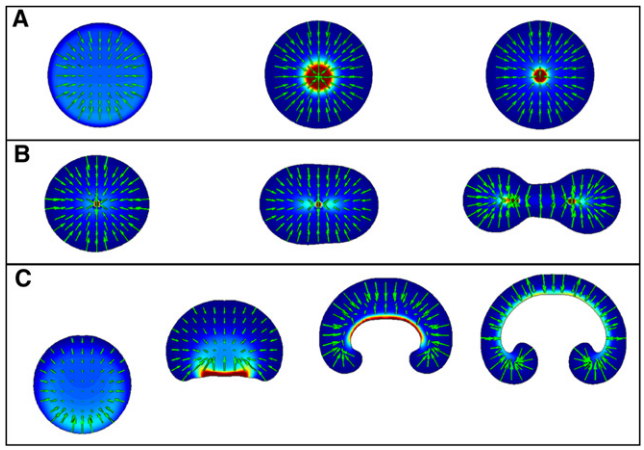

FIGURE 3 Evolution of the actomyosin contraction model for three different sets of parameters. The color maps show the concentration of bound myosin (*blue*, low concentration; *red*, high concentration) and the arrows show the actin flow field. (*A*) When myosin stress is small, the cell remains circular and the myosin is swept to the center of the cell by a centripetal flow of actin. (*B*) At larger values of the myosin stress coefficient, the cell pinches at the center. (*C*) When myosin inhibits protrusion by bundling actin, and the actin viscosity is low, the cell initially takes on a keratocyte-like appearance with a high concentration of myosin at the rear and a half-moon shape. However, this shape does not persist and the cell extends sideways and gets very thin. Simulations use the parameter values listed in the text, except for (*A*) $\eta = 0.3$; (*B*) $\eta = 0.1$; and (*C*) $\alpha = 4$, $\eta = 0.05$, and $\sigma_0 = 0.1$ (Movie S4, Movie S5, and Movie S6).

In this situation, the substrate drag dominates and the effect from myosin is highly localized. For large initial gradients in the myosin concentration, it is possible to obtain a contractile velocity that can pull the rear forward. The initial stages of the simulation look fairly good, with the cell becoming somewhat half-moon-shaped. However, polymerization away from the high myosin concentration continues to spread the cell out, and the cell becomes very wide and thin (Fig. 3 *C*).

These results are intriguing because the model seems to accurately describe the behavior of a keratocyte fragment before the symmetry breaks, in which case the actin cytoskeleton and presumably other factors that influence motility remain fairly isotropic. However, this simple model is incapable of producing a steadily moving cell, which suggests that some other factors are missing. In the following sections, we consider two possible additions to the model that can produce steady crawling: 1), incorporating a graded actin treadmill in which cell polarity is defined by an asymmetric protrusion rate; and 2), using the previously described Rac/Rho model to regulate the actomyosin contraction model.

The actomyosin contraction mechanism stabilizes the motile cell when it is coupled with the graded actin treadmill

In recent experiments, Barnhart et al. (23) examined keratocyte motility on substrates where the adhesive strength was modified, and reported that at low adhesion, the actin polymerization rate appeared to be high at the front of the cell and low at the rear, for unknown reasons. We decided to explore whether adding graded actin protrusion to the actomyosin contraction model could produce keratocyte-like motility in the regime where parameters $f \leq 1$and $\varepsilon \sim 1$. We redefined the boundary velocity to be $\mathbf{v}_b = (V_p(\theta)/(1 + \alpha m) + \mathbf{v}\cdot\mathbf{n})\mathbf{n}$, where the protrusion velocity is $V_p(\theta) = 1 + \beta\, cos\,\theta$, as indicated in the model description.

We first considered the case in which $\alpha = 0$ (myosin does not affect actin polymerization). If the myosin stress is also equal to zero, the cell moves as a disk. Constant polymerization of actin at the cell edge produces centripetal flow of actin into the center of the cell; however, drag between the actin and the substrate slows the flow of actin with respect to the cell motion, and the bound myosin is swept to a location that lags behind the cell center (Fig. 4 *A*). Increasing the myosin stress causes the back of the cell to cave in slightly (Fig. 4 *B*) and also speeds up the cell motion (Fig. 4 *C*). Myosin-mediated acceleration of the cell is in agreement with previously reported measurements (20). However, purely increasing the myosin stress term is insufficient to produce a realistic half-moon shape. We added back in the tendency for myosin to bundle the actin and thereby reduce the protrusion rate by increasing the value of α. The reduction in protrusion at higher concentrations of myosin leads

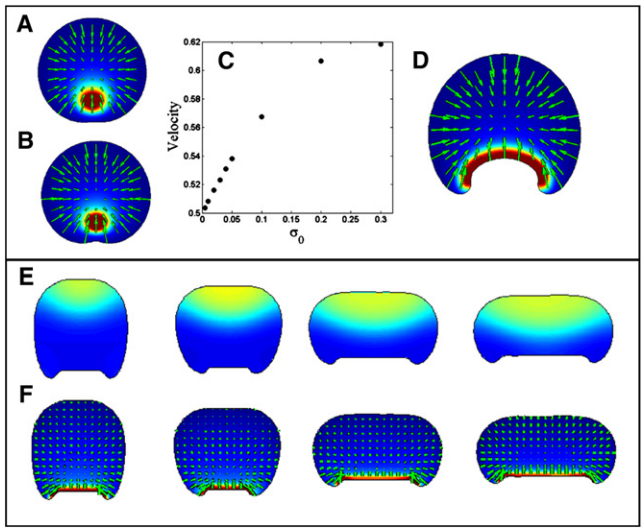

FIGURE 4 (*A–D*) Actomyosin model with a graded actin treadmill. (*A* and *B*) When actin protrusion is independent of myosin concentration, the cell maintains a nearly circular shape. Increasing the myosin stress coefficient leads to a small buckling of the cell rear that increases with increased stress. Simulations use typical parameter values, with values of $\beta = 0.5$ and $\sigma_0 = 0.02$ (*A*) and 0.3 (*B*). (*C*) The stress from myosin also causes the cell to crawl faster. (*D*) When myosin alters actin protrusion, it is possible to obtain a steadily translating, realistic half-moon shape, with actin flows and myosin localization similar to those observed in experiments. Parameter values: $\beta = 0.7$, $\alpha = 0.3$, $\eta = 0.2$, $k_{off} = 0.2$, $k_{on} = 0.2$, and $\sigma_0 = 0.05$. The color map shows the myosin concentration, and green arrows show the actin flow field (Movie S7, Movie S8, and Movie S9). (*E* and *F*) Combined actomyosin contraction and Rac/Rho model. For some parameter values, the cell achieves a steady, crawling half-moon shape. In this simulation, $\alpha = 1$, $\eta = 0.1$, $k_{off} = 0.5$, $k_{on} = 0.5$, and $\sigma_0 = 0.1$. The color map shows the concentrations of active Rac (*E*) and bound myosin (*F*), and the arrows show the actin flow field (Movie S10).

to reduced protrusion of the actin at the rear of the cell. Therefore, the myosin is not swept away from the rear, and accumulates there. It is then possible to find parameter regimes that produce steadily translocating, half-moon shapes with realistic actin flows (6,22,23) and myosin distribution (Fig. 4 *D*). The stable realistic motile cell shape evolves if the scaling of the actin network viscosity, adhesion strength, and myosin stress is such that $f \sim 1$ and $\varepsilon \sim 1$. First, this means that the characteristic distance $(\eta/\zeta)^{1/2}$ on which mechanical stress spreads in the cell is of the order of the cell size, which parallels recent modeling and measurements of the actomyosin contraction in the cell cortex (39). Second, this means that the myosin stress resisted by adhesion generates actin flow at the rear that has to be comparable to the actin polymerization rate at the front.

The actomyosin contraction mechanism also stabilizes the motile cell when coupled with the Rac/Rho model

The results presented above suggest that the myosin contraction model can work to produce steady, crawling

keratocyte shapes as long as an additional polarization mechanism is present. The actin treadmill is an imposed polarization. One possible self-polarizing mechanism is the spontaneous polarization of Rac and Rho. Therefore, we put the actomyosin system under the control of Rac and Rho model that we examined earlier. As before, we assumed high concentrations of active Rac corresponding to low concentrations of Rho. We then assumed that the protrusion rate of actin was proportional to the concentration of active Rac (i.e., the protrusion rate is [Rac]/$(1 + \alpha m)$), and the myosin stress was proportional to the concentration of active Rho (i.e., the myosin stress is σ_0[Rho]m). We found that, for a range of values around the typical parameter values of the actomyosin contraction model, regulation by the simple Rac/Rho model was sufficient to produce a steadily translocating, half-moon-shaped cell (Fig. 4, *E* and *F*). In these simulations, a small perturbation in the initial conditions produced a high concentration of active Rac at the front of the cell and consequently a high concentration of active Rho at the rear. The cell began to crawl by stretching out in the direction of motion and becoming concave at the rear. As the cell continued to crawl, it slowly widened and became more half-moon-shaped. The crawling persisted for a long time but slowed down somewhat because the widening of the cell brought the rear closer to the front, where a high concentration of active Rac was found.

Parameter values significantly different from the default ones did not lead to stable, persistent motion. In all of these cases, morphological changes caused the Rac concentration to become uniform in either the active or inactive state. When this occurred, a radial flow of actin eventually was produced that swept the myosin to the center of the cell, and the cell stopped moving. Sometimes this would happen quickly, and the cell would not move much at all over the course of a simulation. In other simulations, the cell would crawl for a period of time, but then the Rac concentration would flip into one of the two stable states and the cell would then stop moving (Fig. S4).

We also found situations in which the cell would crawl steadily, but there were periodic oscillations at the leading edge of the cell. These were observed when the myosin on and off rates were large and the viscosity was low. Periodic oscillations in motile keratocytes were reported previously (23), and it is not out of the question that our model provides an explanation for these observations.

DISCUSSION

Previous studies provided rigorous proof of the existence of motile cell-like shapes in characteristic cell motility models (40); however, the local and global stabilities of such stationary motile shapes have not been investigated systematically. Here, we show numerically that a wide class of motile models can reproduce stable cell shapes, and that the level set method is a robust tool for simulating the dynamics of motile cells. In the future, as quantitative details of the molecular mechanisms that govern cell migration become clear, it will be easy to couple more mathematical models with the existent ones and rigorously explore the resulting dynamics. We plan to implement the codes of this work within the user-friendly framework of the Virtual Cell (41), so that investigators in the modeling and biology communities will be able to test which combinations of motile models drive the migration of specific cell types.

The main findings of this work are summarized in Table S1 for the reader's convenience. Our main goals in this study were to introduce conceptually novel models of cell shaping by G-actin and microtubule-based transport, and to investigate whether existent models of actin-myosin contraction and Rac/Rho-regulation can predict stable two-dimensional cell shape, separately or in combination. We have demonstrated that three simple mechanisms—spatial grading of the protrusion-limiting G-actin concentration due to diffusion, negative feedback between Rac and Rho resulting in the mutually exclusive assembly of two different kinds of dynamic cytoskeletal structures, and delivery of membrane components via microtubule-limiting protrusion—can reproduce stable lamellipodial shape and movement. The aspect ratio of the characteristic half-moon shape is remarkably insensitive to the model parameters and is of the same order of magnitude as that observed in motile keratocyte cells (25). We have shown that a model in which myosin contracts the actin cytoskeleton can by itself predict globally unstable shapes. This is a novel (to our knowledge) and interesting conclusion, because the idea that actomyosin contraction can be the principal mechanism for cell shaping was suggested previously (19,20) and qualitatively makes perfect sense. Previous numerical simulations on fixed cell shapes (21,22) cast doubt on the ability of this mechanism alone to stabilize the cell shape, but this issue was never investigated fully and consistently. However, we also found that when this model is coupled with either a graded actin treadmill or Rac/Rho regulation, it can predict robust and stable keratocyte-like motility.

Which of the four simulated models are actually relevant to keratocyte motility? It is known that microtubules are not necessary for keratocyte movements (42), but the possibility that biochemical regulation models play a role cannot be definitively ruled out. Of interest, our simple biochemical regulation model does not work properly with the area-preservation term, whereas in keratocytes the area preservation due to membrane inextensibility seems to be important (25). All other models considered in this study work well with, and in fact require, area preservation terms. There is an experimental hint that the G-actin concentration by itself is not the key factor in regulating motility, because the cytoplasm simply contains too much actin in monomeric form (43). Rather, partitioning of the G-actin in a number of forms marked by the hydrolysis state and actin-binding

proteins can, in addition to diffusion, regulate motility. Finally, quantitative data (23) suggest that the actomyosin contraction model complements the graded actin treadmill in shaping the motile cell.

The important question about keratocyte polarization and motility initiation remains open. The available data (37,38) suggest that myosin and perhaps Rac/Rho activity are essential for the observed spontaneous symmetry breakage of the disc-like stationary cell and evolution of the motile half-moon lamellipodium. Of interest, in agreement with those observations, our results suggest that the myosin contraction and Rac/Rho regulation models have properties of both the stationary, nonmotile state (i.e., they are unstable) and the polarized motile state (i.e., they evolve spontaneously). On the other hand, the G-actin and microtubule transport models need additional mechanisms to impose front–back polarization for steady motility to occur.

In an insightful qualitative analysis, Lämmermann and Sixt (7) pointed out that various spatial-temporal combinations of three processes—protrusion, contraction, and adhesion—can be used by the cell to adapt to any two- or three-dimensional environment and to produce any mode of locomotion that has been observed. To do so, the cell has to deploy various combinations of redundant motility models. Here we considered four such models and showed that they can shape and stabilize the motile cell separately or in combination. In this study we did not consider additional models, such as the dynamic graded adhesion treadmill, that have only recently begun to be quantified (44). We plan to add such models to our repertoire, after which quantitative examination of the motile machinery in its entirety will be within reach.

SUPPORTING MATERIAL

Eleven movies, additional text, four figures, two tables, and references are available at http://www.biophysj.org/biophysj/supplemental/S0006-3495(11)00761-2.

We thank K. Keren for useful discussions.

This work was supported by the National Institutes of Health (GLUE grant, Cell Migration Consortium, NIGMS U54 GM64346 to A.M. and C.W., and U54 RR022232 to C.W.) and the National Science Foundation (DMS-0315782 to A.M. and PHY-0749959 to C.W.).

Author contributions: C.W.W. and A.M. designed the research, C.W.W. and J.S. performed the research, and C.W.W. and A.M. wrote the article.

REFERENCES

1. Even-Ram, S., and K. M. Yamada. 2005. Cell migration in 3D matrix. *Curr. Opin. Cell Biol.* 17:524–532.
2. Parri, M., M. L. Taddei, …, P. Chiarugi. 2009. EphA2 reexpression prompts invasion of melanoma cells shifting from mesenchymal to amoeboid-like motility style. *Cancer Res.* 69:2072–2081.
3. Ridley, A. J., M. A. Schwartz, …, A. R. Horwitz. 2003. Cell migration: integrating signals from front to back. *Science.* 302:1704–1709.
4. Mogilner, A. 2009. Mathematics of cell motility: have we got its number? *J. Math. Biol.* 58:105–134.
5. Pollard, T. D., and G. G. Borisy. 2003. Cellular motility driven by assembly and disassembly of actin filaments. *Cell.* 112:453–465.
6. Rafelski, S. M., and J. A. Theriot. 2004. Crawling toward a unified model of cell mobility: spatial and temporal regulation of actin dynamics. *Annu. Rev. Biochem.* 73:209–239.
7. Lämmermann, T., and M. Sixt. 2009. Mechanical modes of 'amoeboid' cell migration. *Curr. Opin. Cell Biol.* 21:636–644.
8. Mogilner, A., and K. Keren. 2009. The shape of motile cells. *Curr. Biol.* 19:R762–R771.
9. Lee, J., A. Ishihara, …, K. Jacobson. 1993. Principles of locomotion for simple-shaped cells. *Nature.* 362:167–171.
10. Satulovsky, J., R. Lui, and Y.-L. Wang. 2008. Exploring the control circuit of cell migration by mathematical modeling. *Biophys. J.* 94:3671–3683.
11. Stéphanou, A., E. Mylona, …, P. Tracqui. 2008. A computational model of cell migration coupling the growth of focal adhesions with oscillatory cell protrusions. *J. Theor. Biol.* 253:701–716.
12. Rubinstein, B., K. Jacobson, and A. Mogilner. 2005. Multiscale two-dimensional modeling of a motile simple-shaped cell. *Multiscale Model Simul.* 3:413–439.
13. Shao, D., W. J. Rappel, and H. Levine. 2010. Computational model for cell morphodynamics. *Phys. Rev. Lett.* 105:108104.
14. Herant, M., and M. Dembo. 2010. Form and function in cell motility: from fibroblasts to keratocytes. *Biophys. J.* 98:1408–1417.
15. Marée, A. F. M., A. Jilkine, …, L. Edelstein-Keshet. 2006. Polarization and movement of keratocytes: a multiscale modelling approach. *Bull. Math. Biol.* 68:1169–1211.
16. Nishimura, S. I., M. Ueda, and M. Sasai. 2009. Cortical factor feedback model for cellular locomotion and cytofission. *PLOS Comput. Biol.* 5:e1000310.
17. Rodriguez, O. C., A. W. Schaefer, …, C. M. Waterman-Storer. 2003. Conserved microtubule-actin interactions in cell movement and morphogenesis. *Nat. Cell Biol.* 5:599–609.
18. Wolgemuth, C. W., and M. Zajac. 2010. The moving boundary node method: a level set-based, finite volume algorithm with applications to cell motility. *J. Comput. Phys.* 229:7287–7308.
19. Prigozhina, N. L., and C. M. Waterman-Storer. 2006. Decreased polarity and increased random motility in PtK1 epithelial cells correlate with inhibition of endosomal recycling. *J. Cell Sci.* 119:3571–3582.
20. Wilson, C. A., M. A. Tsuchida, …, J. A. Theriot. 2010. Myosin II contributes to cell-scale actin network treadmilling through network disassembly. *Nature.* 465:373–377.
21. Mogilner, A., and L. Edelstein-Keshet. 2002. Regulation of actin dynamics in rapidly moving cells: a quantitative analysis. *Biophys. J.* 83:1237–1258.
22. Vallotton, P., G. Danuser, …, A. B. Verkhovsky. 2005. Tracking retrograde flow in keratocytes: news from the front. *Mol. Biol. Cell.* 16:1223–1231.
23. Barnhart, E. L., K.-C. Lee, …, J. A. Theriot. 2011. An adhesion-dependent switch between mechanisms that determine motile cell shape. *PLoS Biol.* 9:e1001059.
24. Novak, I. L., B. M. Slepchenko, and A. Mogilner. 2008. Quantitative analysis of G-actin transport in motile cells. *Biophys. J.* 95:1627–1638.
25. Keren, K., Z. Pincus, …, J. A. Theriot. 2008. Mechanism of shape determination in motile cells. *Nature.* 453:475–480.
26. Bretscher, M. S. 2008. On the shape of migrating cells—a 'front-to-back' model. *J. Cell Sci.* 121:2625–2628.
27. Howes, M. T., M. Kirkham, …, R. G. Parton. 2010. Clathrin-independent carriers form a high capacity endocytic sorting system at the leading edge of migrating cells. *J. Cell Biol.* 190:675–691.

28. Dujardin, D. L., L. E. Barnhart, …, R. B. Vallee. 2003. A role for cytoplasmic dynein and LIS1 in directed cell movement. *J. Cell Biol.* 163:1205–1211.

29. Ridley, A. J., H. F. Paterson, …, A. Hall. 1992. The small GTP-binding protein rac regulates growth factor-induced membrane ruffling. *Cell.* 70:401–410.

30. Lamarche, N., N. Tapon, …, A. Hall. 1996. Rac and Cdc42 induce actin polymerization and G1 cell cycle progression independently of p65PAK and the JNK/SAPK MAP kinase cascade. *Cell.* 87:519–529.

31. Ridley, A. J., and A. Hall. 1992. The small GTP-binding protein rho regulates the assembly of focal adhesions and actin stress fibers in response to growth factors. *Cell.* 70:389–399.

32. Wöllert, T., A. S. DePina, …, G. M. Langford. 2002. GTPase rho is involved in myosin-II-mediated contraction of pseudo-contractile rings and transport of vesicles in extracts of clam oocytes. *Biol. Bull.* 203:208–210.

33. Mori, Y., A. Jilkine, and L. Edelstein-Keshet. 2008. Wave-pinning and cell polarity from a bistable reaction-diffusion system. *Biophys. J.* 94:3684–3697.

34. Rubinstein, B., M. F. Fournier, …, A. Mogilner. 2009. Actin-myosin viscoelastic flow in the keratocyte lamellipod. *Biophys. J.* 97:1853–1863.

35. Verkhovsky, A. B., T. M. Svitkina, and G. G. Borisy. 1999. Network contraction model for cell translocation and retrograde flow. *Biochem. Soc. Symp.* 65:207–222.

36. Cramer, L. P. 1999. Role of actin-filament disassembly in lamellipodium protrusion in motile cells revealed using the drug jasplakinolide. *Curr. Biol.* 9:1095–1105.

37. Verkhovsky, A. B., T. M. Svitkina, and G. G. Borisy. 1999. Self-polarization and directional motility of cytoplasm. *Curr. Biol.* 9:11–20.

38. Yam, P. T., C. A. Wilson, …, J. A. Theriot. 2007. Actin-myosin network reorganization breaks symmetry at the cell rear to spontaneously initiate polarized cell motility. *J. Cell Biol.* 178:1207–1221.

39. Mayer, M., M. Depken, …, S. W. Grill. 2010. Anisotropies in cortical tension reveal the physical basis of polarizing cortical flows. *Nature.* 467:617–621.

40. Choi, Y., and R. Lui. 2009. Existence of traveling domain solutions for a two-dimensional moving boundary problem. *Trans. AMS.* 361:4027–4044.

41. Slepchenko, B. M., and L. M. Loew. 2010. Use of virtual cell in studies of cellular dynamics. *Int. Rev. Cell Mol. Biol.* 283:1–56.

42. Euteneuer, U., and M. Schliwa. 1984. Persistent, directional motility of cells and cytoplasmic fragments in the absence of microtubules. *Nature.* 310:58–61.

43. Koestler, S. A., K. Rottner, …, J. V. Small. 2009. F- and G-actin concentrations in lamellipodia of moving cells. *PLoS ONE.* 4:e4810.

44. Cirit, M., M. Krajcovic, …, J. M. Haugh. 2010. Stochastic model of integrin-mediated signaling and adhesion dynamics at the leading edges of migrating cells. *PLOS Comput. Biol.* 6:e1000688.

Supplemental Material for "Redundant mechanisms for stable cell locomotion revealed by minimal models" by Charles W. Wolgemuth, Jelena Stajic, and Alex Mogilner

Supplemental Figures

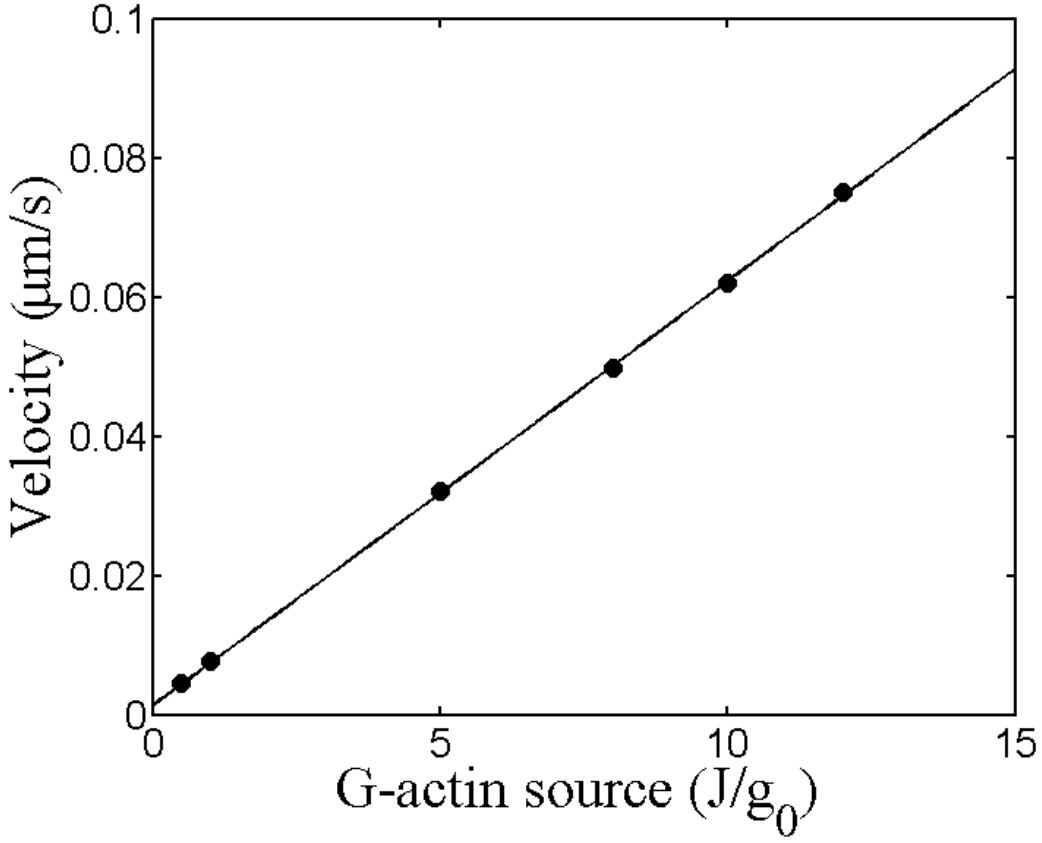

Figure S1 In the G-actin model, crawling speed depends linearly on the depolymerization rate, but is nearly independent of the polymerization rate (not shown).

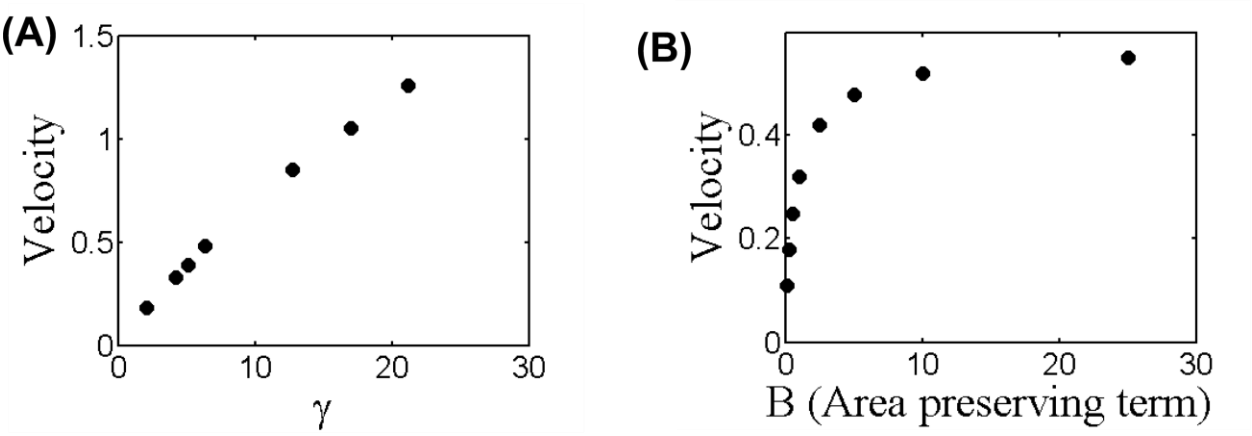

Figure S2 (A-B) The dependence of the crawling speed on the model parameters. The velocity increases roughly linearly with the parameter $\gamma = V_0 N\nu\text{-}/2\pi(\nu_+ + \nu_-)$ and is unaffected by the area preserving term B when B > 5.

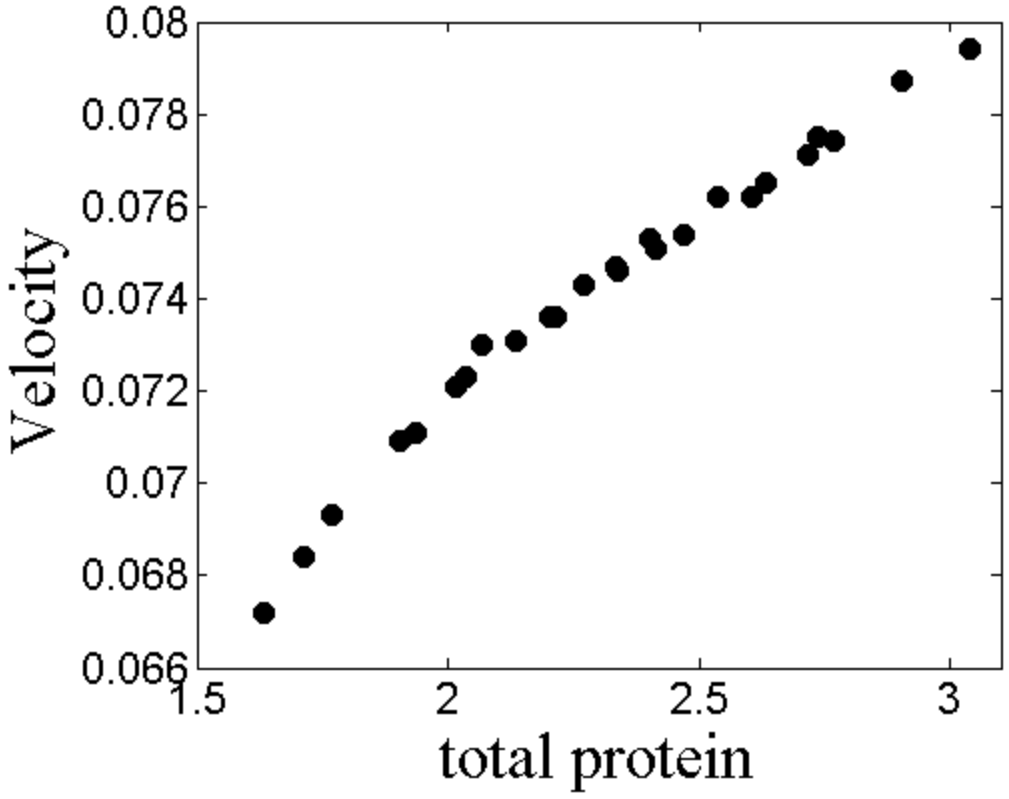

Figure S3 The velocity in the Rac/Rho model increases with the total amount of protein (a+b).

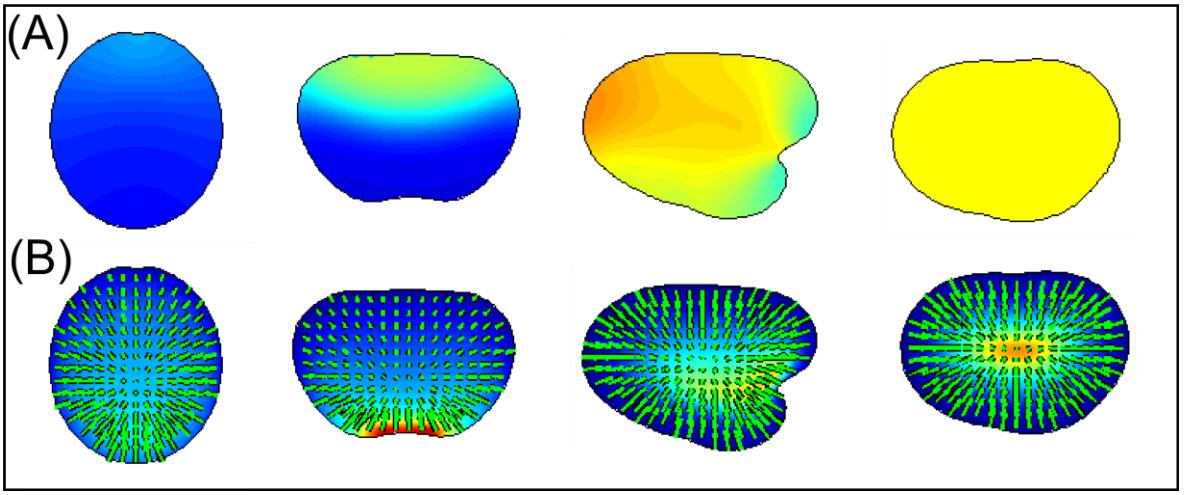

Figure S4 (A,B) For other values of the parameters in the combined actomyosin contraction and Rac/Rho model, the cell crawls for a while, but then reaches a uniform concentration of active Rac, which causes the cell to take on a more radially-driected flow field. In (A) the colormap shows the concentration of active Rac, and in (B) the colormap shows the concentration of bound myosin and the arrows show the actin flow field. In this simulation, $\alpha = 1$, $\eta = 0.2$, $k_{off} = 2.5$, $k_{on} = 2.5$, and $\sigma_0 = 0.1$. See Supplemental Movie 11.

Supplemental Text

In this Supplemental Material section we provide further details on the motivations that lead us to propose the four motility models that we examine, and we describe the mathematical models for each of the four mechanisms presented in the text.

Extended Background. The question of how motile cells maintain shape and speed is partially answered by the 'actin treadmill in the inextensible membrane bag' model proposed by Keren et al (1) for fish keratocyte cells. According to this model, actin filaments are distributed unevenly around the cell periphery, with denser filaments at the front that push the cell boundary forward and generate faster protrusion, while at the sides the less dense filaments are stalled by the membrane tension. The rear of the keratocyte cell is pulled forward by a combination of membrane tension and myosin contraction (2, 3). For many other cells, myosin-generated contraction of the actin network has long been assumed, and in some cases proved, to be the primary force that advances the rear of the cell (4, 5). Importantly, Keren et al (1) found that the keratocyte cell area is constant during motility indicating that the plasma membrane is stretched tight around the lamellipodium constraining the cell shape. The role that the membrane plays in limiting lamellipodial area during crawling remains open for other cells.

The actin treadmill works because away from the leading edge F-actin disassembles and replenishes the pool of G-actin in the cell. G-actin monomers diffuse throughout the cell and polymerize at or near the lamellipodial leading edge. Growth of actin filaments, and therefore extension of the cell boundary, is proportional to the local G-actin concentration, which is not necessarily constant throughout the cell but is determined by a balance of diffusion, reaction, disassembly and assembly processes (6). Qualitatively, the idea that graded G-actin concentration can lead to graded F-actin growth, thereby defining cell shape, was discussed in (1) but never examined quantitatively.

Cell motility is not only mechanical, but is also a biochemical process. Cell shape can be regulated by gradients of signaling molecules in the cytoplasm and on the membrane. For example, the hypothesis that feedbacks between two RhoGTPases, Rac and Rho, lead to mutually exclusive assembly of two different kinds of dynamic cytoskeletal structures, which in turn promotes the establishment of the front–back polarity of such motile cells as neutrophils, has drawn much attention and support (7-9). Last, but not least, microtubules are intimately involved in guiding migrating cells (10) and regulating their shapes (11). Multiple redundant pathways that are not well understood contribute to the microtubule-actin crosstalk (12).

Mathematical models. These models were all solved numerically using the Moving Boundary Node Method (13), which is described briefly at the end of this section. All simulations are non-dimensionalized with respect to a characteristic cell length and we use an initial geometry that is a circular domain with unit radius. All our models are two-dimensional, reflecting the 2D character of the lamellipodia. Simulations were run on a 161x161 Cartesian grid that is 4 x 4 in dimensionless units, and the time step was typically chosen to be less than 0.01 in dimensionless units.

G-actin transport model. In this model, G-actin diffuses through the cell with diffusion coefficient D and polymerizes at a rate proportional to the concentration, $k_{on}g(\mathbf{x})$, where k_{on} is the rate constant and $g(\mathbf{x})$ is the local G-actin concentration. We define the leading edge (i.e., where

polymerization is active) using the vector $\mathbf{x}_{LE}$ to denote the positions of points on the boundary that are part of the leading edge. We assume that F-actin disassembles under the cell body, which is defined to be a circular region that lies just in front of the midpoint of the rear of the cell. The circular depolymerization zone moves with the cell rear being pulled forward by the retracting cell membrane. We define the zone at the rear of the cell where actin does not polymerize in an ad hoc way, introducing a wide ellipse that is centered at the same location as the depolymerization zone. The location of that center moves with the center of the depolymerization zone. Any boundary points that fell within the ellipse has polymerization rate equal to zero; all other boundary points expand with the rate $k_{on}g(x)$. Thus, we assume a constant source of G-actin, $k_{off}H(\mathbf{x})$, where k_{off} is the depolymerization rate and $H(\mathbf{x})$ is a function that is equal to one inside the cell body region and zero outside. The G-actin can also be carried along by the cytosolic velocity **v**. We compute the cytosolic velocity by treating the membrane as impermeable. The velocity of the membrane then defines the normal component of the cytosolic velocity at the boundary. We then set the tangential component of the cytosolic velocity at the boundary using the center of mass velocity of the cell. The cytosolic velocity inside the cell can then be computed to be the smoothest velocity that is consistent with the given velocity on the boundary (method described in (13)). The concentration of G-actin then satisfies the following equation:

$$\frac{\partial g}{\partial t} = D\nabla^2 g - \nabla\cdot\left(g\mathbf{v}\right) - k_{on}g\delta(\mathbf{x}-\mathbf{x}_{LE}) + k_{off}H(\mathbf{x}) \qquad (1)$$

where $\delta(\mathbf{x})$ is the Dirac delta-function. We use a zero flux boundary condition for the G-actin concentration. Mathematically, the sink term on the boundary of the domain is equivalent to specifying a flux of G-actin along x_LE. Both formulations work equally well and give the same result as shown in (6) and (14). Polymerization of G-actin at the boundary pushes the cell forward in the direction normal to the cell boundary. In addition, we assume that the cell has a preferred area A_0 and that deviations from this area produce an effective restoring velocity locally normal to the cell boundary (see more details in the acto-myosin model). Therefore, the velocity of the cell boundary is $\mathbf{v}_b = (\alpha k_{on}g(\mathbf{x})\delta(\mathbf{x}-\mathbf{x}_{LE}) - B(A-A_0)/A_0)\,\mathbf{n}$, where α is a constant that sets the velocity of protrusion in terms of the polymerization rate, B is a constant, and **n** is the normal vector at the boundary. Eq. 1 is non-dimensionalized using the characteristic length of a cell, $L = \sqrt{A_0}$, and the characteristic timescale L^2/D. With this choice of non-dimensionalization, there are two primary parameters, the dimensionless on and off-rates. We start our simulations with a circular domain of unit radius and a uniform concentration of G-actin.

Microtubule-associated vesicle transport model. This model is based on the notion that vesicle transport to the leading edge permits polymerization to push forward the membrane. Vesicles are transported along microtubules, and the flux of these vesicles is assumed to be proportional to the density of microtubule ends at the cell periphery. We model the average density of microtubules using the model described in (15). In this model, microtubules grow with a speed of v_+ and shrink with a speed v_-. Growing microtubules transition to shrinking microtubules at a rate f_-, and shrinking microtubules become growing microtubules at a rate f_+. These rates define a characteristic length scale $r_0 = v_-v_+/(v_-f_+ - v_+f_-)$. If $\bar{N}$ microtubules grow out

from the MTOC, then the average density of microtubule plus ends a distance r away from the MTOC is

$$N(\mathrm{r}) = \frac{\bar{\mathrm{N}}}{2\pi \mathrm{r}} \left(\frac{v_-}{v_+ + v_-} \right) \frac{\mathrm{e}^{-\mathrm{r}/\mathrm{r}_0}}{\mathrm{r}_0} \qquad (2)$$

We set the protrusion velocity to be proportional to the microtubule end density and impose a preferred cell area, A_0, to represent a conservation of the total amount of membrane. The boundary velocity is therefore $\mathbf{v}_b = (V_0 N(\mathrm{r}) - B(A-A_0)/A_0)\,\mathbf{n}$, where V_0 is a parameter normalizing the protrusion rate, A is the actual cell area, B is a constant, and **n** is the normal vector.

Rac/Rho model. We model the Rac and Rho dynamics using a simplified model that was originally proposed in (16). In this model, a conserved number of molecules of a single protein are considered where the protein can be in one of two states, active or inactive. There is assumed to be cooperative positive feedback from the active form onto its own production. Conversion back to the inactive state, however, occurs at a constant basal rate, δ. The positive feedback is modeled using a second order Hill function, with maximal rate γ and saturation parameter K. Since the active protein binds to the cell membrane, the active protein is assumed to diffuse much slower than the cytosolic, inactive form. Both species are also transported with the cytoslic velocity, as in the G-actin model. Denoting the active protein as species *A* and the inactive form as species *B*, with concentrations as *a* and *b*, respectively, the time evolution of the two species is given by

$$\begin{aligned} \frac{\partial a}{\partial \mathrm{t}} &= \mathrm{D}_\mathrm{A} \nabla^2 a - \nabla \cdot (a\mathbf{v}) + \left(\mathrm{k}_0 + \frac{\gamma a^2}{\mathrm{K}^2 + a^2} \right) b - \delta a \\ \frac{\partial b}{\partial \mathrm{t}} &= \mathrm{D}_\mathrm{B} \nabla^2 b - \nabla \cdot (b\mathbf{v}) - \left(\mathrm{k}_0 + \frac{\gamma a^2}{\mathrm{K}^2 + a^2} \right) b + \delta a \end{aligned} \qquad (3)$$

where D_A and D_B are the diffusion coefficients and k_0 is the basal rate of activation. Besides diffusion, the protein is also carried along by the cytosolic velocity **v**, which is determined as in the previous model. We treat species *A* as the active form of Rac, and consider that activated Rho mirrors the behavior of *A* (i.e, where active Rac is at high concentration, active Rho is at low concentration, and vice versa.) The polymerization rate of the actin is considered to be proportional to the concentration of active Rac, and myosin contraction is proportional to Rho. Therefore, the boundary velocity can be written in terms of the concentration of species *A* as $\mathbf{v}_b = V_0(a - a_0)\mathbf{n}/a_0$ where V_0 is a characteristic velocity, and a_0 is the concentration at which Rho-induced contraction exceeds the polymerization-driven protrusion induced by active Rac. In the model, a_0 is a concentration scale that is roughly equal to the average concentration of *A*. For our simulations, we used the kinetic parameters that were defined in (16): $D_A = 0.4\ \mu\mathrm{m}^2/\mathrm{s}$, $D_B = 40\ \mu\mathrm{m}^2/\mathrm{s}$, $\delta = 1\ \mathrm{s}^{-1}$, $\gamma = 1\ \mathrm{s}^{-1}$, $k_0 = 0.067\ \mathrm{s}^{-1}$, and K = 1 (in units normalized by a characteristic concentration). We non-dimensionalize length using a characteristic cell length of $10\,\mu\mathrm{m}$ and start our simulations with a circular domain of unit radius. Note that this model does not work if the area-preservation term is introduced; the steadily moving shape does not evolve. The initial

concentration of B is uniform and the concentration of A was typically chosen to have a small gradient (roughly 10% of the average concentration) in the y-direction. However, we did run simulations with a random initial concentration of A and obtained equivalent results for the steady state shape and speed.

Acto-myosin contraction model. In this model, myosin can bind and unbind from the actin cytoskeleton with rate constants K_{on} and K_{off}, respectively. We define the concentration of bound myosin to be $m(x)$. We assume that the unbound myosin diffuses rapidly compared to the other relevant timescales in the problem. Therefore, we treat the unbound myosin concentration as being uniform throughout the cell. If the total number of myosin molecules in the cell is M_T, then the concentration of unbound myosin is

$$m_u = \frac{1}{A}\left(M_T - \int m dA\right) \tag{4}$$

where A is the area of the cell. Bound myosin exerts an isotropic, contractile stress on the cytoskeleton, which induces a flow in the actin network. This flow, described by the velocity field **v**, carries the bound myosin with it. Therefore, the dynamic equation for the bound myosin is

$$\frac{\partial m}{\partial t} = -\nabla \cdot (m\mathbf{v}) + K_{on} m_u - K_{off} m \tag{5}$$

We treat the actin cytoskeleton as a viscous fluid with viscosity η. The cytoskeleton feels the stress from the bound myosin and also experiences a resistive drag force due to adhesion with the substrate $\mathbf{f}_{drag} = -\zeta \mathbf{v}$, where ζ is treated as a constant. Therefore, local force balance on the cytoskeleton leads to

$$\zeta \mathbf{v} = \nabla \cdot \left(\frac{\eta}{2}\left(\nabla \mathbf{v} + (\nabla \mathbf{v})^T\right) + \sigma_0 m \hat{\mathbf{I}} \right) \tag{6}$$

The right-hand side of Eq. 6 is the divergence of the total stress on the actin cytoskeleton. The first term is the viscous stress tensor and the last term is the stress due to the myosin with σ_0 a constant coefficient that determines the stress per myosin motor. $\hat{\mathbf{I}}$ is the identity matrix. Eq. 6 is non-dimensionalized by dividing by the drag coefficient times a characteristic velocity, V_0, and Eq. 5 is non-dimensionalized by dividing by a characteristic myosin concentration and multiplying by the timescale L/V_0, where $L = \sqrt{A_0}$ is the size of the cell. We assume that the cell has a preferred area A_0 set by the total stretched area of the plasma membrane. Deviations upward from this area generate a membrane tension that stalls actin polymerization and allows contraction to bring the area down. Deviations downward allow free actin polymerization to expand the cell back to the preferred area. We model this situation by the boundary conditions on Eq. 6 such that the total stress is equal to $B(A-A_0)/A_0$. We used the non-dimensional value B = 20 in our simulations. Though a stress boundary condition for a viscous fluid can lead to indeterminacy in the solution (i.e., it is a Neumann condition), the resistive drag force between the actin and the substrate that is proportional to the velocity removes this degeneracy from the equation.

At the boundary of the cell, the F-actin is swept inward due to the contraction of the network by the myosin motors. In addition, the F-actin polymerizes at the boundary, pushing the boundary outward in the direction of the boundary normal **n**. The net velocity of the boundary is the sum of these two contributions. We therefore define the boundary velocity to be equal to the normal component of the actin velocity at the boundary plus a polymerization velocity. We assume that the high concentrations of bound myosin bundle the actin, thereby reducing the polymerization rate. The boundary velocity is then $\mathbf{v}_b = (V_0/(1+\alpha m) + \mathbf{v}\cdot\mathbf{n})\mathbf{n}$, where V_0 is the rate of actin polymerization in the absence of myosin and α is a constant. The bound myosin is advected (as is shown in Eq. (5)) with the velocity of the actin, which is computed using Eq. (6), and we use a zero flux boundary condition to prevent myosin from entering or leaving through the boundary.

The Moving Boundary Node Method. We use a level set-based, finite volume routine to solve numerically the moving boundary problems that are described in this paper (13). Briefly, this method describes the cell boundary using a signed distance map. The distance map defines the distance to the nearest point on the boundary at all points in space, with negative values inside the cell and positive values outside the cell. Therefore, the zero contour of this distance map is the boundary. The method uses a standard method for evolving the distance map in time, given the boundary velocity (17, 18). The distance map is also used to construct an accurate discretization of the cell geometry, by moving Cartesian grid nodes that neighbor the zero contour of the distance map directly onto the boundary. The displacement of the nodes in this fashion allows us to construct a second-order accurate finite volume discretization of the cell. This discretization is then used to evolve the concentrations and velocities in time using a Crank-Nicolson-type scheme.

The use of a signed distance map to describe boundary provides an implicit definition of the boundary; i.e., material points on the boundary are not explicitly defined. Therefore, the distance map does not contain information about how far two material points on the boundary move away from one another during a time step. Additional calculations would be necessary to calculate the local tension in the membrane due to stretching. However, lipid bilayers are largely inextensible, and the tension in the membrane is largely set by the availability (or lack thereof) of additional membrane. The tension in the membrane can be approximated by a global parameter. The pressure that the membrane exerts back on the cell is proportional to the tension times the curvature. The level set method allows one to easily calculate geometric properties of the membrane, such as the curvature, with second order accuracy. Under these conditions, the level set method provides an accurate method for handling the forces due to the cell membrane.

1. Keren K*, et al.* (2008) Mechanism of shape determination in motile cells. *Nature* 453:475-480.
2. Rubinstein B, Fournier MF, Jacobson K, Verkhovsky A, & Mogilner A (2009) Actin-myosin viscoelastic flow in the keratocyte lamellipod. *Biophys. J.* 97:1853-1863.
3. Barnhart EL, Lee K-C, Keren K, Mogilner A, & Theriot JA (2011) An adhesion-dependent switch between mechanisms that determine motile cell shape. *PLoS Biol.* 9:e1001059.
4. Verkhovsky AB, Svitkina TM, & Borisy GG (1999) A network contraction model for cell translocation and retrograde flow. *Biochem. Soc. Symp.* 65:207-222.
5. Vallotton P, Danuser G, Bohnet S, Meister J-J, & Verkhovsky AB (2005) Tracking retrograde flow in keratocytes: news from the front. *Mol. Biol. Cell* 16:1223-1231.
6. Novak IL, Slepchenko BM, & Mogilner A (2007) Quantitative analysis of G-actin transport in motile cells. *Biophys. J.* 95:1627-1638.

7. Xu J*, et al.* (2003) Divergent signals and cytoskeletal assemblies regulate self-organizing polarity in neutrophils. *Cell* 114:201-214.
8. Wong K, Pertz O, Hahn K, & Bourne H (2006) Neutrophil polarization: spatiotemporal dynamics of RhoA activity support a self-organizing mechanism. *Proc. Natl. Acad. Sci. USA* 103:3639-3644.
9. Narang A (2006) Spontaneous polarization in eukaryotic gradient sensing: a mathematical model based on mutual inhibition of frontness and backness pathways. *J. Theor. Biol.* 240:538-553.
10. Small JV, Geiger B, Kaverina I, & Bershadsky A (2002) How do microtubules guide migrating cells? *Nat. Rev. Mol. Cell Biol.* 3:957-964.
11. Picone R*, et al.* (2010) A polarised population of dynamic microtubules mediates homeostatic length control in animal cells. *PLoS Biol.* 8:e1000542.
12. Rodriquez OC*, et al.* (2003) Conserved microtubule-actin interactions in cell movement and morphogenesis. *Nat. Cell Biol.* 5:599-609.
13. Wolgemuth CW & Zajac M (2009) The moving boundary node method: a level set-based, finite volume algorithm with applications to cell motility. *J. Comput. Phys.*:(submitted).
14. Mogilner A & Edelstein-Keshet L (2002) Regualtion of actin dynamics in rapidly moving cells: a quantitative analysis. *Biophys. J.* 83:1237-1258.
15. Dogterom M & Leibler S (1993) Physical aspects of the growth and regulation of microtubule structures. *Phys. Rev. Lett.* 70:1347-1350.
16. Mori Y, Jilkine A, & Edelstein-Keshet L (2008) Wave-pinning and cell polarity from a bistable reaction-diffusion system. *Biophys. J.* 94:3684-3697.
17. Fedkiw RP, Aslam T, Merriman B, & Osher S (1999) A non-oscillatory eulerian approach to interfaces in multimaterial flows (the ghost fluid method). *J. Comput. Phys.* 152:457-492.
18. Adalsteinsson D & Sethian JA (1999) The fast construction of extension velocities in level set methods. *J. Comput. Phys.* 148:2-22.

Supplemental Table 1: main findings of this study.

Model and its conceptual novelty	Nature of the cell-shaping mechanism	Reproduces characteristic stable shape of the motile cell?	Mechanism works with membrane-area limiting factor?	Mechanism causes self-polarization
G-actin transport (conceptually novel)	Transport-limited	Yes, robustly	Yes	No, cell has to be polarized by another mechanism
Microtubule-associated vesicle transport (conceptually novel)	Transport-limited	Yes, robustly	Yes	No, cell has to be polarized by another mechanism
Rac/Rho (not conceptually novel)	Biochemical regulation	Yes, robustly	No	Yes
Actomyosin contraction (not conceptually novel)	Mechanical	No, shape is unstable	N/A	Yes
Hybrid actomyosin contraction + Rac/Rho (conceptually novel)	Mechano-chemical	Yes, but only when mechanical parameters are fine-tuned	No	Yes
Hybrid actomyosin contraction + Graded actin treadmill (conceptually novel)	Mechano-chemical	Yes, but only when mechanical parameters are fine-tuned	Yes	Depends on the level of desciption

Supplemental Table 2: Description of the model paramters.

G-actin Model	Description	Dimensionless form	Characteristic value
D	G-actin diffusion coefficient	N/A	1
k_{on}	polymerization rate of F-actin	$k_{on}L^2/D$	2
k_{off}	F-actin depolymerization rate	$k_{off}L^2/Dg_0 = J/g_0$	5
g_0	characteristic G-actin concentration	N/A	1
α	velocity coefficient	$\alpha g_0/L$	0.1
L	characteristic cell size	N/A	1
B	Area constraint strength		10
Microtubule Model			
γ	polymerization velocity constant	see text	10
r_0	microtubule length scale	see text	0.53
B	Area constraint strength		10
Rac/Rho Model			
D_A	Diffusion coefficient for species A	$D_A/L^2\delta$	0.004
D_B	Diffusion coefficient for species B	$D_B/L^2\delta$	0.4
A_0	characteristic concentration of species A	N/A	1
δ	deactivation rate	N/A	1
γ	nonlinear activation rate	$\gamma A_0^2/\delta$	1
k_0	basal activation rate	k_0/δ	0.067
K	saturation parameter	K/A_0^2	1
V_0	velocity coefficient	V_0L/D	0.1
a_0	velocity transition concentration	a_0/A_0	0.684
Actomyosin Model			
k_{on}	rate constant for myosin binding to actin	$k_{on}L/V_0$	0.25
k_{off}	myosin dissociation rate constant	$k_{off}L/V_0$	0.5
ζ	drag coefficient for movement of actin against the substrate	$\Omega = \zeta V_0 L^3$	1
η	F-actin viscosity	$\varepsilon = \eta/\zeta L^2$	0.2
σ_0	coefficient relating myosin concentration to actin	$\sigma_0 M_T/L^2$	0.2

	contractile stress		
M_T	Total number of myosin molecules in cell	M_T	4π
L	characteristic cell size	L	1
B	area constraint parameter	B	20
V_0	characteristic polymerization velocity	V_0	1
α	parameter that determines the effect of bound myosin on the polymerization velocity	α	1